Polymer 51 (2010) 4969–4977

Contents lists available at ScienceDirect

Polymer

journal homepage: www.elsevier.com/locate/polymer

Morphology, microstructure and compatibility of impact polypropylene copolymer

Chunhui Zhang [a,b], Yonggang Shangguan [a,b,*], Ruifen Chen [a,b], Yuanzhi Wu [a,b], Feng Chen [a,b], Qiang Zheng [a,b,*], Guohua Hu [c,d]

[a] Key Laboratory of Macromolecular Synthesis and Functionalization, Ministry of Education, Hangzhou 310027, PR China
[b] Department of Polymer Science and Engineering, Zhejiang University, Hangzhou 310027, PR China
[c] Laboratory of Reactions and Process Engineering, Nancy-Université, CNRS-ENSIC-INPL, 1 rue Grandville, BP 20451, 54001 Nancy, France
[d] Institut Universitaire de France, Maison des Universités, 103 Boulevard Saint-Michel, 75005 Paris, France

ARTICLE INFO

Article history:
Received 15 April 2010
Received in revised form
21 June 2010
Accepted 9 August 2010
Available online 15 August 2010

Keywords:
Impact polypropylene copolymer (IPC)
Successive self-nucleation and annealing (SSA)
Fractionation

ABSTRACT

The morphology of impact polypropylene copolymer (IPC) was studied through scanning electron microscope (SEM) and transmission electron microscope (TEM) observation, and a modified dispersed phase model of IPC with core-shell structure was proposed. Through fractionation of IPC, the glass transitions of the ethylene–propylene random copolymer (EPR) fraction, ethylene–propylene block copolymer (E*b*P) fraction and propylene homopolymer (*i*PP) fraction were detected, respectively. Moreover, the glass transitions and crystallization behaviors of E*b*P/*i*PP and EPR/E*b*P fraction blends were systemically investigated and several reasonable chain structures of E*b*P component were confirmed. The results reveal that the E*b*P component presents three glass transition peaks, and the glass transition temperature of ethylene–propylene random copolymer in IPC sample is remarkably lower than that of pure EPR fraction due to the existence of special structure of E*b*P component in IPC. In addition, co-crystallization occurring between the polypropylene chains in E*b*P fraction and in *i*PP fraction was found for solution-mixed E*b*P/*i*PP blends, and it is believed that there exists a dilute effect of EPR on the crystallization of E*b*P fraction for the solution-mixed EPR/E*b*P blends. Accordingly, it can be inferred that E*b*P fraction has good compatibility with both EPR and *i*PP fraction, and indeed it confirms that the compatibilization effect of E*b*P fraction in IPC was good.

1. Introduction

Due to its excellent impact property, impact polypropylene copolymer (IPC) has attracted researchers' great attention in the past two decades [1–3]. Because it is prepared by two-step polymerization, bulk polymerization of propylene and then gas-phase copolymerization of ethylene and propylene, IPC should be denoted as a multi-component '*alloy*' in nature. Some researches on IPC have demonstrated the complexity of composition and morphology of IPC. According to these experimental results, IPC mainly contains three compositions, *i.e.*, ethylene–propylene random copolymer (EPR), a series of ethylene–propylene block copolymers with different sequence lengths (E*b*P) and propylene homopolymer (*i*PP) [1,2,4–10].

By means of ultramicrotomy and atomic force microscope (AFM), Tanem et al. observed a complex dispersed particle morphology in IPC [11]. Recently, we proposed a primary dispersed particle model with core-shell structure in IPC using AFM, X-ray diffraction (XRD), dynamic mechanical analysis (DMA) and differential scanning calorimetry (DSC). The dispersed phase is composed of EPR and some ethylene–propylene copolymer (E*b*P). In this dispersed particle model, EPR and the crystallizable PP segments in E*b*P component forms the shell, and the crystallizable PE segments are major part of the core [12]. In addition, Yang et al. [13] studied the multilayered core-shell structure of the dispersed phase in IPC and Feng et al. [14] probed the influence of shear on crystallization of IPC and proposed a complex dispersed particle model with core-shell structure to describe the mechanism of shear-enhanced crystallization. However, after investigating the chain structure and morphology of IPC recently, we found the

* Corresponding authors. Department of Polymer Science and Engineering, Zhejiang University, Hangzhou 310027, PR China. Tel./fax: +86 571 8795 2522.
E-mail addresses: shangguan@zju.edu.cn (Y. Shangguan), zhengqiang@zju.edu.cn (G. Zheng).

0032-3861/$ – see front matter © 2010 Elsevier Ltd. All rights reserved.
doi:10.1016/j.polymer.2010.08.021

Table 1
Molecular weight and fraction amount for IPC and its fractions.

Sample	Fraction amount (%)	$M_n \times 10^4$	$M_w \times 10^4$	PD
IPC	–	4.39	17.4	3.96
EPR fraction	18.96	8.45	22.7	2.68
E*b*P fraction	11.30	1.60	18.0	11.25
*i*PP fraction	69.74	4.60	15.1	3.28

above mentioned phase-structure models cannot give a satisfactory explanation on the morphology of the dispersed phase of IPC.

Since the compatibility between components is important to multi-component polymeric material and the matrix and main dispersed phase of IPC are *i*PP and EPR respectively, investigation of the compatibility between these two components is one of the key steps to understand structure–property relationship of IPC. Moreover, because of the existence of E*b*P, it is essential to learn the interaction between E*b*P and EPR as well as E*b*P and *i*PP. We have compared two different IPCs and found that IPC with higher E*b*P content had a better impact-resistance [15]. In addition, some other researches also indicated that E*b*P may enhance the compatibility between EPR and *i*PP component in IPC [1,16]. However, the direct evidence on the compatibilization effect of E*b*P component was seldom provided.

Recently, we have studied the chain structure of the components of the IPC by thermal analysis and proposed the reasonable macromolecular structures of E*b*P component [17]. In the present article, we try to put forward a modified phase model for IPC based on the chain structure analysis to better understand the morphology of IPC. In addition, we will also investigate the miscibility/compatibility between the components of IPC, especially the compatibilization effect of E*b*P component to EPR and *i*PP components, in order to understand the compatibilization effect of E*b*P component for the other two components in IPC.

2. Experimental

2.1. Materials and sample preparation

The commercial IPC (SP179) was purchased from SINOPEC Qilu Corporation Ltd., China. The IPC was fractionated through temperature-gradient extraction fractionation method and *n*-octane was used as the solvent to successively extract the sample at different temperatures. Firstly, 25 g origin IPC resin was completely dissolved in *n*-Octane at 125 °C. Subsequently, the solution was cooled down to 50 °C and held for 72 h at the same temperature, and the fraction was collected as *EPR fraction*. Then, the remaining sample was extracted at 100 °C for 72 h and the collected fraction was named as *EbP fraction*. After the above two-step extraction, the remainder was the third fraction, *iPP fraction*. The molecular weight of IPC, the weight ratio of the fractions and the molecular weight of the fractions were listed in Table 1.

Two blend samples, *i*PP/E*b*P and E*b*P/EPR, were prepared by solution-mixed method, respectively. Firstly, the fractions to be mixed were weighted according to the designated proportion, and they were dissolved in boiling xylene. Subsequently, the solution was mixed with excessive methanol to participate. After filtration, the blends of the fractions were obtained and then dried in vacuum at 80 °C for 24 h.

2.2. DSC analysis

The thermal behavior was examined by using a Q100 MDSC (TA Instruments Corporation, USA) with nitrogen as purge gas. The samples were heated to 200 °C and held for 10 min to eliminate previous thermal history before testing. Except for special explanation, the cooling and heating rate were 10 °C/min.

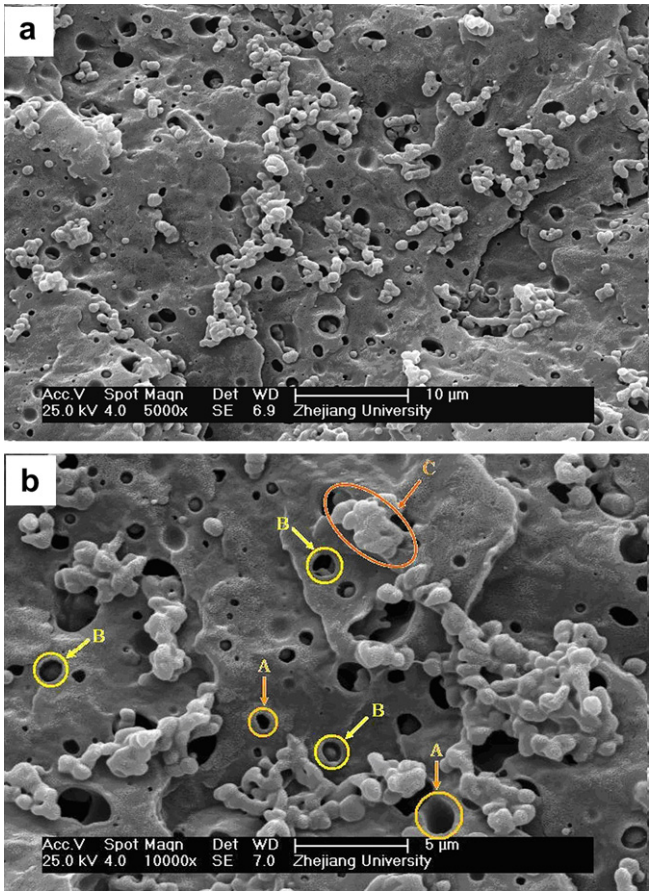

Fig. 1. SEM micrographs of fracture surface of the IPC in different magnifications.

Successive self-nucleation and annealing (SSA) [18] was performed according to the following procedure: the samples were first preheated at 200 °C for 10 min and then cooled down to 30 °C at a constant cooling rate of 10 °C/min and held at this temperature for 1 min, and subsequently, the SSA treatment was started. As is introduced in literatures [19–21], the first self-seeding temperature (T_s) in SSA course should be the temperature at which almost all the polymer crystals have been melted and only small crystal fragments that could act as self-nuclei was left. After the self-nucleation experiments [21], 169 °C was chosen as the first T_s for blends of *i*PP/E*b*P, and 154 °C, for the blends of E*b*P/EPR. The fractionation window adopted here was 5 °C and the annealing time was 10 min. The scanning rate during the thermal conditioning steps was 10 °C/min. For the *i*PP/E*b*P samples, the temperature range of the thermal fractionation was from 124 to 169 °C, and for the E*b*P/EPR, was from 89 to 154 °C. After the SSA treatment, the melting traces were recorded at a heating rate of 10 °C/min.

2.3. Dynamic mechanical analysis

The DMA measurements were carried out on a Q800 Dynamic Mechanical Analyzer (TA Instruments Corporation, USA). A film tension mode was used for the temperature sweep under a heating rate of 3 °C/min and a frequency of 10 Hz. The film specimens were prepared by compression molding at 170 °C.

2.4. Scanning electron microscope (SEM) observation

Fracture surface of IPC specimens obtained at liquid nitrogen was etched in xylene for 15 h at room temperature, and was observed

using a scanning electron microscope (SEM) (SIRION, FEI, Netherland) after being coated with gold–palladium. The operating voltage was 25 kV, and the magnifications were 5000 and 10,000, respectively.

2.5. Transmission electron microscope (TEM) observation

The as-received IPC sample was dissolved in boiling xylene with a concentration of 0.05 wt%. Then, a thin film for TEM observation was prepared by solution-casting to the preheated copper grids. After being dried in vacuum at 80 °C for 3 h, the film was heated to 200 °C, and kept isothermally for 10 min in nitrogen atmosphere. An EM-430 (Philips, Netherlands) transmission electron microscope operated at 300 kV was used for observation.

3. Results and discussion

3.1. Phase structure of IPC

Fig. 1 gives the SEM images of the fracture surface for IPC after being etched by xylene. It is seen from Fig. 1a that a two-phase structure with uniform dispersion exists. However, it can be found in an enlarged micrograph of this morphology shown in Fig. 1b that the dispersed phase indeed presents three different cases: (i) isolated holes marked as '*A*', (ii) the holes but containing a smaller granule marked as '*B*', and (iii) aggregate granules marked as '*C*'.

In our previous work, the chain structure of E*b*P component of IPC has been probed by nuclear magnetic resonance (NMR) and DSC [15]. The result suggested that the chains of E*b*P component contain not only crystallizable polyethylene and polypropylene segment, but also some ethylene–propylene random sequences. Recently, we further studied the chain structure of E*b*P component of IPC by thermal analysis and proposed four kinds of E*b*P chain structures [17]. Based on the chain structure model of E*b*P and morphology observation, we propose a modified phase model of IPC as shown in Fig. 2. In this model, the dispersed phase is composed of an E*b*P core and two layers, and the outer layer is E*b*P and the inner one is EPR. In particular, some E*b*Ps pass through the EPR layer and form some bridges connecting the core and E*b*P layer. Four kinds of E*b*P chains are marked as I, II, III and IV, respectively. The chains dominated by polypropylene segments are denoted as type I, and they tend to locate in the interface layer between *i*PP matrix and EPR dispersed phase, taking a role of compatiblizer. The chains dominated by polyethylene segments are denoted as type II, and they tend to locate inside EPR dispersed phase to form the PE-rich core. The chains with equivalent PP or PE content are denoted as type III, and they are indeed '*block copolymer*' and may locate in E*b*P layer or core, even stay across the EPR shell to form the E*b*P bridge. The chains containing some ethylene–propylene random sequences are denoted as type IV, and they may stay anywhere of E*b*P components. When the IPC sample is etched by the xylene, and in which the EPR shells are solved, the E*b*P cores completely wrapped by EPR layer are removed, and the E*b*P cores with weaker E*b*P bridges are also removed. As a result, the holes form on the fracture surface, indicated by arrows '*A*' in Fig. 1b. However, for the dispersed phase where the PE-rich cores are not totally wrapped by the EPR shell, the cores may still remain and form the holes with a smaller granule, being indicated by arrows '*B*' in Fig. 1b. When the dispersed particles get together and the outer E*b*P layers result in an invalid etch of xylene, the aggregation of dispersed particles can be observed on the fracture surface, as shown by arrows '*C*' in Fig. 1b.

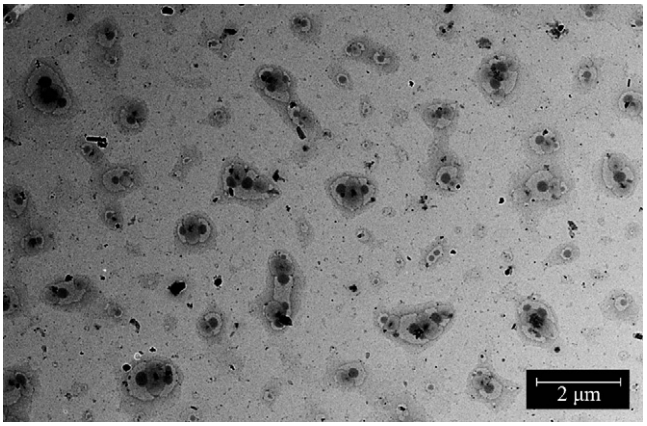

Fig. 3. TEM micrograph of IPC solution-casting film.

Fig. 3 gives the TEM image of the solution-casting film of IPC after being annealed at 200 °C for 10 min. It can be seen that there exists a two-phase structure with good dispersion, and the dispersed particles exhibit a clear multilayered core-shell structure including a dark inner core, a dark outer ring and a light intermediate layer. The core-shell structure of the dispersed particles of the IPC film prepared by solution-casting has been well studied by selected area electron diffraction (SAED) [13,14]. According to the

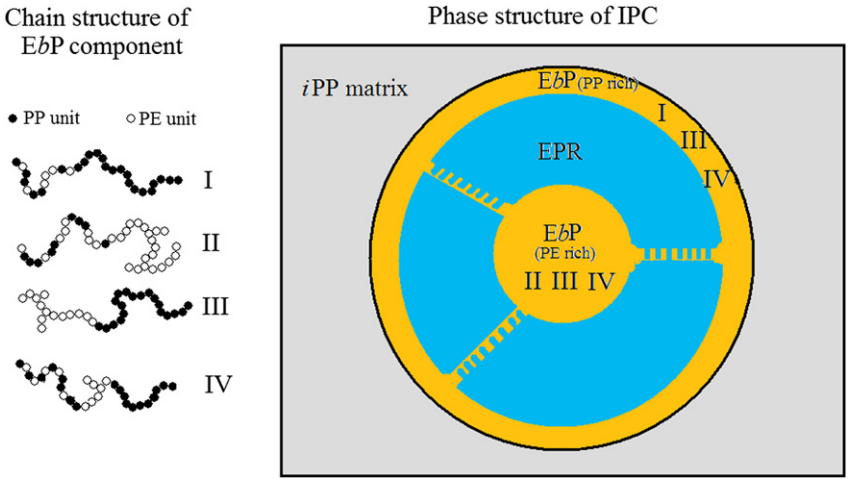

Fig. 2. Schematic diagrams for chain structure of E*b*P component and phase structure of IPC.

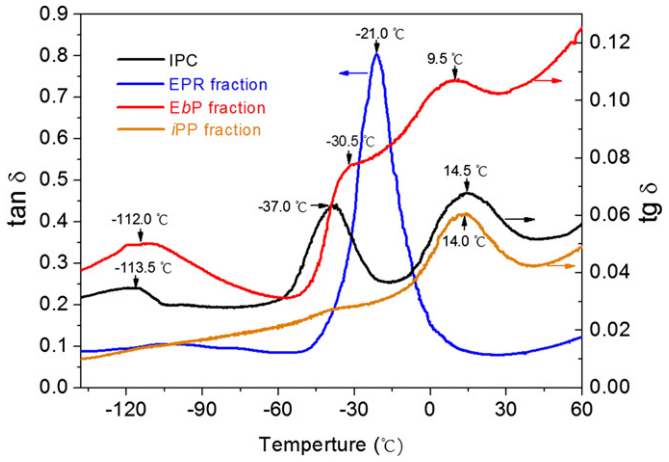

Fig. 4. Temperature dependence of tan δ for IPC and its fractions at a frequency of 10 Hz and a heating rate of 3 °C/min.

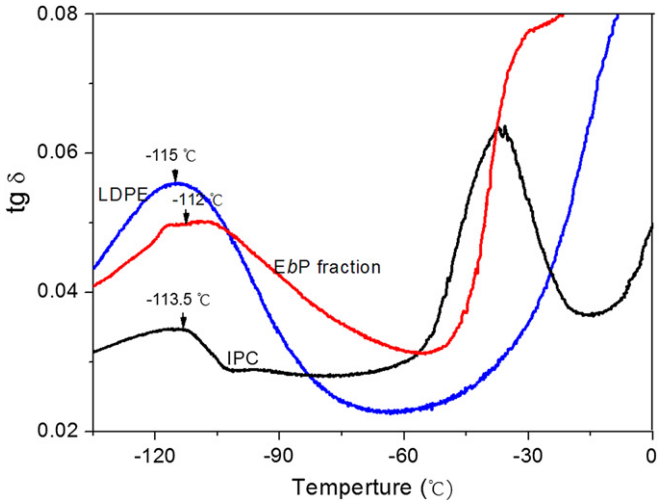

Fig. 5. Temperature dependence of tan δ for IPC and LDPE at a frequency of 10 Hz and a heating rate of 3 °C/min.

SAED result, the dark inner core comprises PE crystals formed by PE homopolymer and its long blocks, the dark outer ring comprises PE crystals formed by segmented ethylene–propylene copolymer and the light intermediate layer mainly consists of ethylene–propylene random copolymer. In our previous work, the morphology in bulk for the same IPC product was examined by AFM [12]. It can be found that the morphology of IPC film prepared by solution-casting is quite like that of IPC in bulk. This result implies that the multilayered core-shell structure is the thermodynamic stable structure for the dispersed phase of IPC; even this structure is completely destroyed by dissolving the IPC in xylene, it can be rebuilt by a process like self-assembly.

It is noted that the particle size of the dispersed phase is from 0.5 to 2.5 μm for the IPC. Jang et al. [22] proposed that 0.5 μm is a critical particle diameter of elastomer and only the rubber particles with larger dimensions than the critical diameter could promote crazing and improve the fracture resistance of polymeric materials. Obviously, the sizes of dispersed particles in IPC are almost beyond this critical dimension. In addition, a broader distribution of rubber particle size also facilitates improving the impact toughness of the IPC. Hence, it is believed that the excellent toughness of IPC results from the good dispersion and appropriate size of EPR.

3.2. Glass transition behavior of IPC and its fractions

Fig. 4 gives the dependences of tan δ on temperature for IPC and its different fractions. It can be seen that for both IPC and E*b*P fraction, there are three tan δ peaks. However, for the *i*PP and EPR fractions, single peak appears. The single peak of *i*PP fraction at 14 °C clearly belongs to glass transition of propylene homopolymer, and that of EPR fraction at −21 °C, to glass transition of ethylene–propylene random copolymer. Considering the above results, the peaks of IPC located at about −37 and 14.5 °C should be ascribed to glass transitions of EPR and *i*PP, respectively, in accordance with previously reported results [23,24]. However, the peak located at about −113.5 °C in IPC has never been reported in previous literature. Since a peak with similar temperature also appears on the tan δ plot of E*b*P fraction, it is suggested that this peak of IPC at −113.5 °C results from the existence of E*b*P fraction. Fig. 5 gives the temperature dependence of tan δ for low density polyethylene (LDPE) as well as the tan δ for IPC and E*b*P fraction. There exists an obvious glass transition peak at around −115 °C for LDPE and it approaches those observed in IPC and E*b*P fractions, indicating that the tan δ peaks at −112 °C for E*b*P fraction indeed corresponds to the glass transition of the polyethylene component. The previous results demonstrated that the E*b*P fraction mainly consists of crystallizable ethylene–propylene segmented copolymer and an independent PE crystallization could be observed when the ethylene segment in some segmented copolymer is long enough [3,15,25,26]. Similarly, the observed PE glass transition peak indicates that in E*b*P polymer chains, some ethylene segments are long enough to enable their glass transition peak to appear. In addition, the two tan δ peaks which are located at −30.5 and 9.5 °C are ascribed to ethylene–propylene random copolymer and propylene homopolymer, respectively.

It is well accepted that EPR in IPC is the main component acting as impact modifier in IPC and the excellent impact-resistance property of IPCs at low temperatures is related to low T_g of EPR component. It is interesting that even the EPR transition peaks of both IPC and EPR fraction reflect the transition of the same component, the two T_gs are different as shown in Fig. 4, *i.e.*, T_g of EPR component in IPC is remarkably lower than that of pure EPR sample. It is reasonable that other components in IPC should exert an influence on T_g of EPR component. Since there is little heterogeneity in EPR fraction, the −21 °C should be the real T_g of EPR component. The lowering of T_g of EPR in IPC should be attributed to the influence of PE-rich component with a much lower T_g, because in a temperature range over T_g of PE-rich E*b*P component and below T_g of EPR component, the free volume in the PE-rich E*b*P component expands with the increase of temperature. Due to the good compatibility of these two adjacent components, the free volume for EPR molecules also increases. As a result, the T_g of EPR component decreases. For the similar reason, the T_g of EPR observed in E*b*P fraction is also lower than that of EPR fraction, as shown in Fig. 4. However, T_g of EPR in E*b*P fraction is higher than that in IPC, which can be interpreted as follows: In E*b*P fraction, there are stronger interactions between macromolecular chains, and, as a result, T_g of EPR increases due to the PP segment exerting much obvious influence on EPR segment; in contrast, the *i*PP component has a weak influence on the T_g of EPR in IPC because the two components are divided by E*b*P component. For the same reason, the T_g of PP in E*b*P is 5 °C lower than that in IPC. These results are believed to be another proof supporting the E*b*P structure proposed in Fig. 2.

3.3. Glass transition behavior of EPR/EbP and EbP/iPP blends

For multi-component polymers, the T_g change of each component could indicate certain interaction or compatibility between

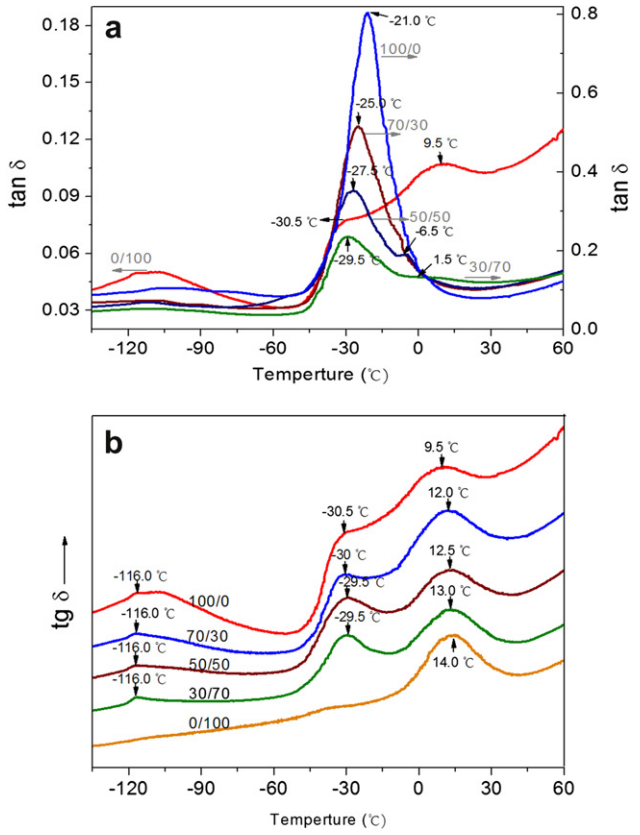

Fig. 6. Temperature dependence of tan δ for blends of the fractions at a frequency of 10 Hz and a heating rate of 3 °C/min for (a) EPR/E*b*P blends and (b) E*b*P/*i*PP blends.

components to some level [27,28]. Hence, the T_g decrease of EPR component in IPC means that the EPR fraction and E*b*P fraction are partially compatible at least. It is necessary to further study the interaction between two fractions. Fig. 6a gives the dependences of tan δ on temperature for solution-mixed EPR/E*b*P blends with different compositions. For EPR/E*b*P with 30/70 composition, two glass transition peaks at −29.5 and 1.5 °C can be observed. The low temperature peak is ascribed to the glass transition of EPR while the other to the propylene homopolymer. However, the glass transition of polypropylene is weak and unobvious, and its T_g is 8 °C lower than that in pure E*b*P. For the composition of 50/50, two glass transition peaks can still be observed, but the transition peak of polypropylene is even weaker, and a T_g decrease of more than 10 °C could be found compared to pure E*b*P fraction. For EPR/E*b*P with 70/30 composition, only a single glass transition peak can be observed. In addition, T_gs of EPR for all the samples are located between T_g (−30.5 °C) of EPR for E*b*P fraction and that (−21 °C) of EPR fraction, and these T_gs present a regular change with the composition variation. These results confirm that the EPR and E*b*P fractions have a good compatibility.

Fig. 6b shows the temperature-dependence of tan δ for solution-mixed E*b*P/*i*PP blends with various compositions. It can be seen that all blends demonstrate three glass transition peaks, among which there appear no change for two transition peaks at about −116 °C and −30 °C corresponding to glass transition of polyethylene and random ethylene-propylene copolymer, respectively. However, it is quite interesting that the glass transition peak of ethylene–propylene random copolymer becomes clearer with the increase of *i*PP content. The reason for this may be that when E*b*P fraction is mixed with *i*PP fraction, the crystallization ability of E*b*P

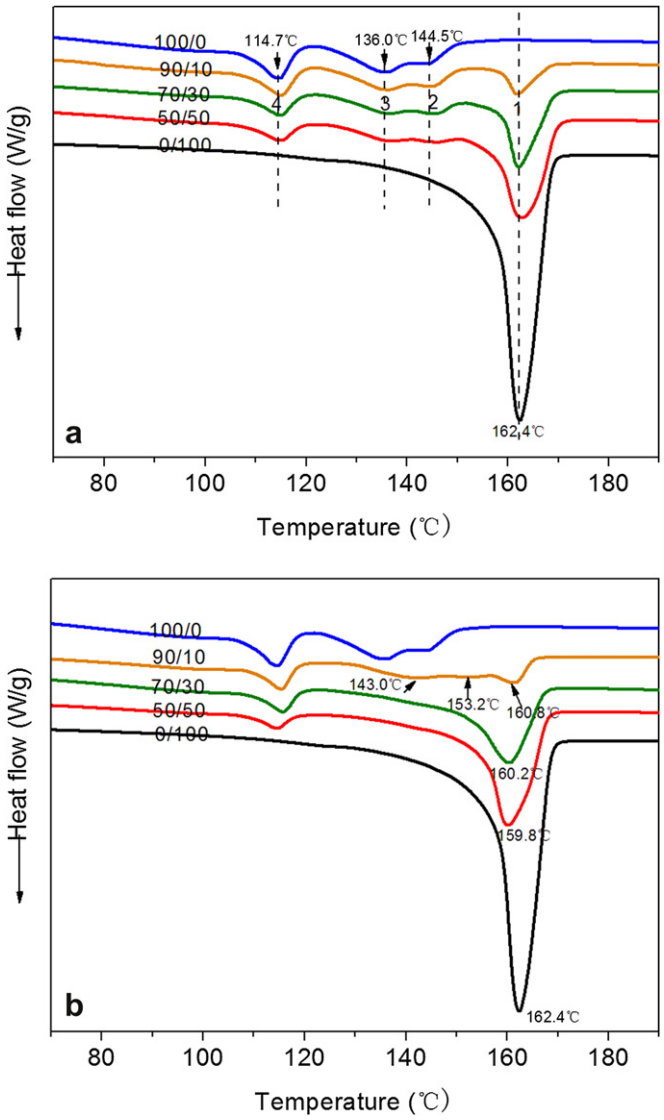

Fig. 7. DSC melting traces for blends of E*b*P and *i*PP fractions at a heating rate of 10 °C/min for (a) unmixed samples and (b) solution-mixed samples.

fraction is enhanced, and, as a result, the EPR transition peak in the blends becomes clearer compared with that of pure E*b*P fraction, because the glass transition of some macromolecular chains whose T_gs are located between the transition peak of EPR and PP component either is weakened or may appear at a higher temperature. The interaction between the two fractions will be further discussed in the next section. Furthermore, the T_gs of PP appear at 12 °C, 12.5 °C and 13 °C for blends with different compositions, respectively, and all T_g are higher than the corresponding T_g of E*b*P fraction and slightly lower than that of *i*PP fraction. Due to the difference of T_g of PP between pure *i*PP and E*b*P fraction is no more than 5 °C, the change of T_g of PP in blends could hardly be accepted as stronger evidence for their interaction.

3.4. Crystallization of EbP/iPP blends

Fig. 7a shows the DSC heating traces of pure E*b*P, *i*PP fractions and their '*unmixed samples*' after they crystallize from 200 °C at a cooling rate of 10 °C/min. Here, the so called '*unmixed sample*' is the one in which two components never contact with each other inside DSC crucible. It can be seen that the pure *i*PP fraction exhibits

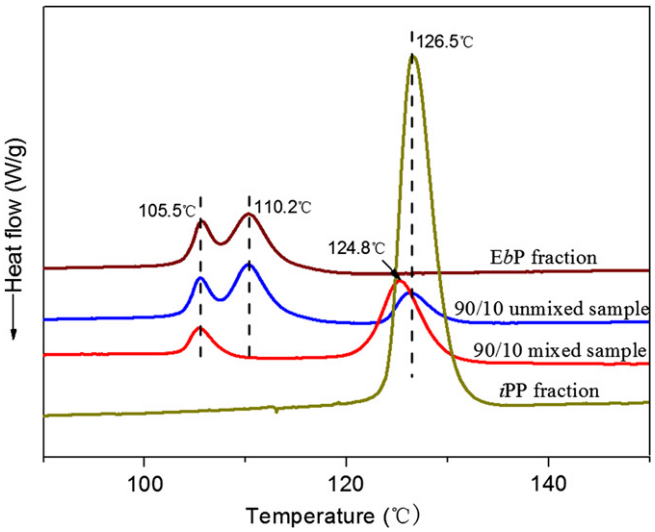

Fig. 8. DSC cooling traces for E*b*P fraction, *i*PP fraction as well as unmixed and solution-mixed E*b*P/*i*PP samples at a cooling rate of 1 °C/min.

one sharp melting peak located at 162.4 °C, and the pure E*b*P fraction, however, exhibits three melting peaks located at about 144.5 °C, 136.0 °C and 114.7 °C, respectively. The melting peak at 114.7 °C is attributed to the melting of polyethylene crystals formed by crystallizable ethylene segments, in agreement with our previous work [17]. Considering the character of E*b*P fraction, both peaks located at 144.5 and 136.0 °C should be attributed to the melting of the polypropylene crystals with relatively low lamellae thickness. The thin lamellae of the polypropylene crystals results from the embedding of the ethylene units in the crystallizable propylene chain segments. These ethylene units act as defects and reduce the lamellae thickness of polypropylene crystals. Moreover, the two polypropylene melting peaks in a broad temperature range also indicate that the E*b*P fraction comprises polypropylene segments with non-uniform perfection degrees.

There exist four melting peaks for the unmixed E*b*P/*i*PP samples, in which three melting peaks in lower temperatures are attributed to E*b*P fraction and the other at highest temperature, to *i*PP component. Basically, the area of each melting peak is proportional to the weight ratio of corresponding component, indicating that two fractions in blends never influence each other during cooling and heating process.

Fig. 7b shows heating traces of pure E*b*P, *i*PP and their solution-mixed blends after being crystallized from 200 °C at a cooling rate of 10 °C/min. For the solution-mixed blends with compositions of 50/50 and 70/30, only two melting peaks appear, compared with four peaks of the unmixed E*b*P/*i*PP samples with the same composition. Although the area and temperature of polyethylene melting peaks for solution-mixed blends are almost the same as those of the unmixed samples with the same composition, the number of melting peaks for polypropylene decrease from three to one. In addition, the melting peak temperatures of polypropylene for the solution-mixed blends with composition of 50/50 and 70/30 are at 159.8 °C and 160.2 °C, respectively, which are much higher than those of polypropylene crystals in pure E*b*P fraction and a bit lower than that of pure *i*PP fraction. These results imply that some interactions exist between E*b*P and *i*PP component in solution-mixed blends, and, as a result, the melting peaks of polypropylene crystals with relatively low lamellae thickness disappear.

There exist four melting peaks for the solution-mixed sample with composition of 90/10, in which two melting peaks at 153.2 °C and 143.0 °C should be attributed to the polypropylene crystals

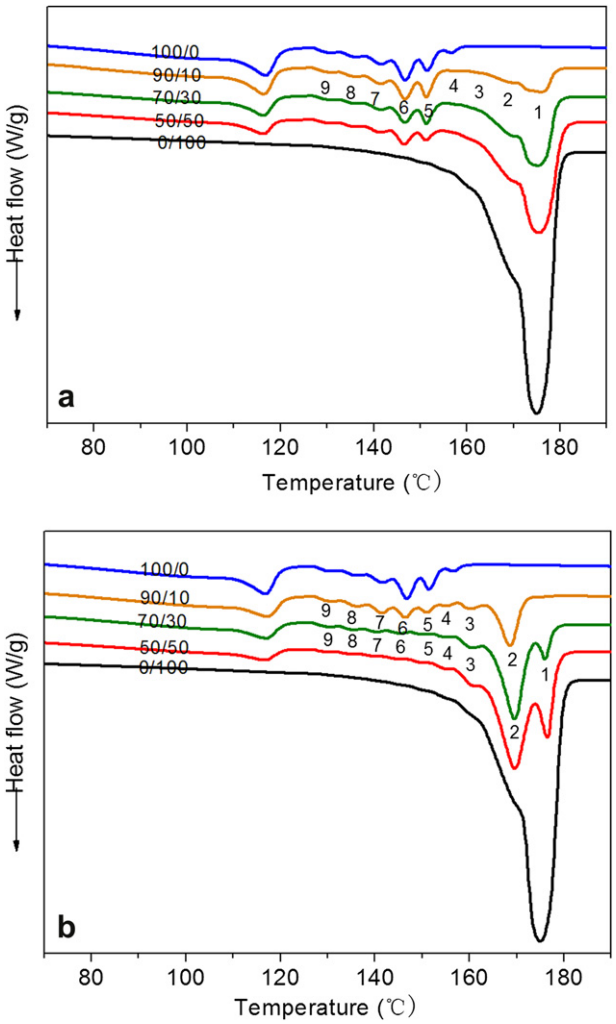

Fig. 9. DSC melting traces at a heating rate of 10 °C/min for blends of E*b*P and *i*PP fractions after SSA treatment for (a) unmixed samples and (b) solution-mixed samples.

with relatively low lamellae thickness. However, the temperatures of these melting peaks are much higher than those of the unmixed sample with the same composition. These results also suggest that there exists interaction between E*b*P and *i*PP fractions.

Fig. 8 gives the cooling trace of E*b*P fraction, *i*PP fraction as well as the unmixed and solution-mixed E*b*P/*i*PP samples with composition of 90/10. It can be seen that E*b*P fraction presents two exothermic peaks. Take its composition into account, the peak at 105.5 °C should be attributed to the crystallization of PE, and the peak at 110.2 °C, to the crystallization of PP. On the other hand, the *i*PP fraction exhibits only a single exothermic peak at 126.5 °C, corresponding to the crystallization of propylene homopolymer. It can also be found that the unmixed and mixed E*b*P/*i*PP samples are present in different traces. For the unmixed E*b*P/*i*PP sample, three exothermic peaks appear and they should be separately ascribed to the crystallization of the two fractions. In contrast, only a single crystallization peak of PP could be found on the cooling trace of the mixed sample.

It is thought that the difference of the heating and cooling behaviors for the mixed and unmixed samples results from two factors: one is the induced crystallization effect of *i*PP fraction on the crystallizable polypropylene segments in E*b*P fraction, and the *i*PP fraction plays the role of nucleation agent to E*b*P fraction so that both the corresponding crystallization and melting temperatures increase; the other is that the existence of *i*PP fraction enhances

crystallization ability of the polypropylene segments in E*b*P fraction to form co-crystals between two fractions because of their good compatibility.

It is noted that the simple heating and cooling processes could hardly distinguish the attributions of the above two factors. Hence, successive self-nucleation and annealing (SSA) is adopted to further investigate the interaction mechanism of the two fractions, and it is accepted that SSA is an effective thermal fractionation technique and can gain more information on the crystallization course. Fig. 9a shows the melting traces of unmixed E*b*P/*i*PP samples with various compositions after being subjected to a ten-step SSA treatment with a 5 °C decrease per step from 169 °C to 124 °C. It can be found that pure *i*PP fraction is difficult to be fractionated due to the low defects content, while the fractionation effect is obvious for the E*b*P fraction and samples containing E*b*P fraction. Moreover, the peak at the highest temperature is caused by the melting of *i*PP crystals formed by the polymer chain with the lowest defects concentration. For the E*b*P/*i*PP blends with composition of 90/10, 70/30 and 50/50, the melting peaks labeled as 1–3 should come from the *i*PP fraction, and other melting peaks labeled as 4–9 are from E*b*P fraction. The results could be expected because no interaction exists between two components in the unmixed samples.

Fig. 9b shows the DSC melting traces of solution-mixed E*b*P/*i*PP blends with various compositions after being subjected to the SSA treatment. It can be seen that although the number of melting peaks for blends with composition of 70/30 and 50/50 are the same as compared with the unmixed E*b*P/*i*PP samples, obvious difference in the intensity of the melting peaks appears. For example, the intensity of the melting peak at the highest temperature (peak 1) of the solution-mixed samples is much lower than that of the unmixed samples with the same composition, while its melting peak (peak 2) is obviously stronger. Furthermore, for the mixed sample with composition of 90/10, the peak at the highest temperature seems to have disappeared. Hence, this phenomenon should not be interpreted as nucleating effect, and the occurrence of co-crystallization between polypropylene chains in E*b*P fraction and in *i*PP fraction is believed to be more reasonable.

The polypropylene co-crystallization between two fractions may also support the previous interpretation on the EPR glass transition in E*b*P/*i*PP blends shown in Fig. 6b, *i.e.*, with increase of *i*PP fraction, more polypropylene chain segments in E*b*P fraction participate in co-crystallization and results in the decrease of the free volume, and as a result T_g of some molecular chains from E*b*P fraction shifts towards high temperature and the transition peak of EPR becomes clearer.

3.5. Crystallization of EPR/EbP blends

It has been reported that the ethylene–propylene random copolymer could crystallize at certain conditions [29,30]. It has also been found in our previous work that there exists a poor crystallization ability of EPR fraction in IPC because the fraction contains tiny crystallizable ethylene or propylene sequences [17]. Hence it is necessary to measure the crystallization behavior of the blends containing EPR and E*b*P fractions to examine their compatibility. Fig. 10a gives the melting traces of unmixed samples of EPR/E*b*P fraction with different compositions. The pure EPR fraction exhibits two weak but broad exothermic peaks at about 32.0 °C and 79.5 °C, respectively. The number and shape of the melting peaks for all the unmixed samples are similar. However, these peaks are difficult to be observed when the amount of EPR is lower than that of E*b*P because the melting peaks of the EPR fraction are weak.

Fig. 10b depicts the melting traces of solution-mixed blends of EPR/E*b*P fraction with different compositions. The solution-mixed blends exhibit some different characteristics compared with the unmixed EPR/E*b*P samples, *e.g.*, two melting peaks at lower temperatures only appear for pure EPR sample, indicating the existence of crystallization. Fig. 10c gives comparison between the melting traces of unmixed and mixed samples with composition of 70/30. Five melting peaks labeled as 1–5 appear for the unmixed sample, in

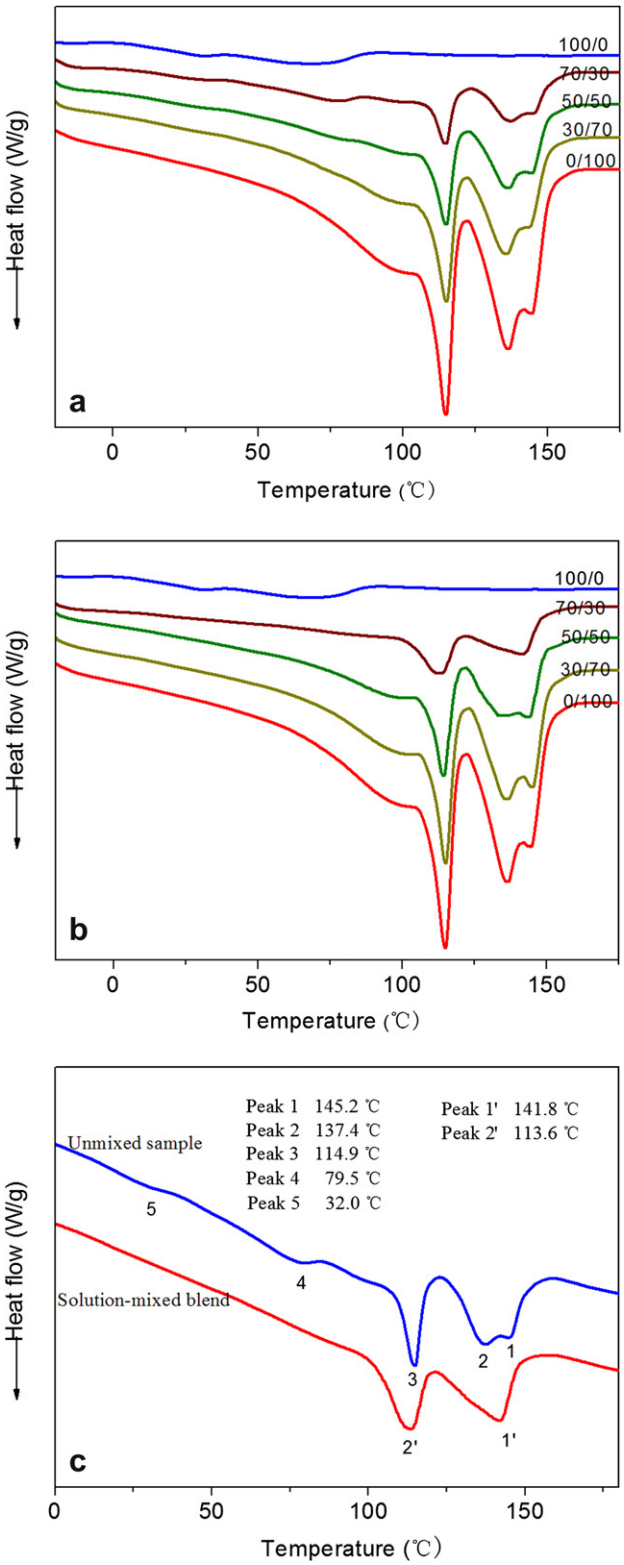

Fig. 10. DSC melting traces for blends of EPR and E*b*P fractions at a heating rate of 10 °C/min for (a) unmixed samples, (b) solution-mixed samples and (c) comparison of the unmixed and the mixed samples with composition of 70/30.

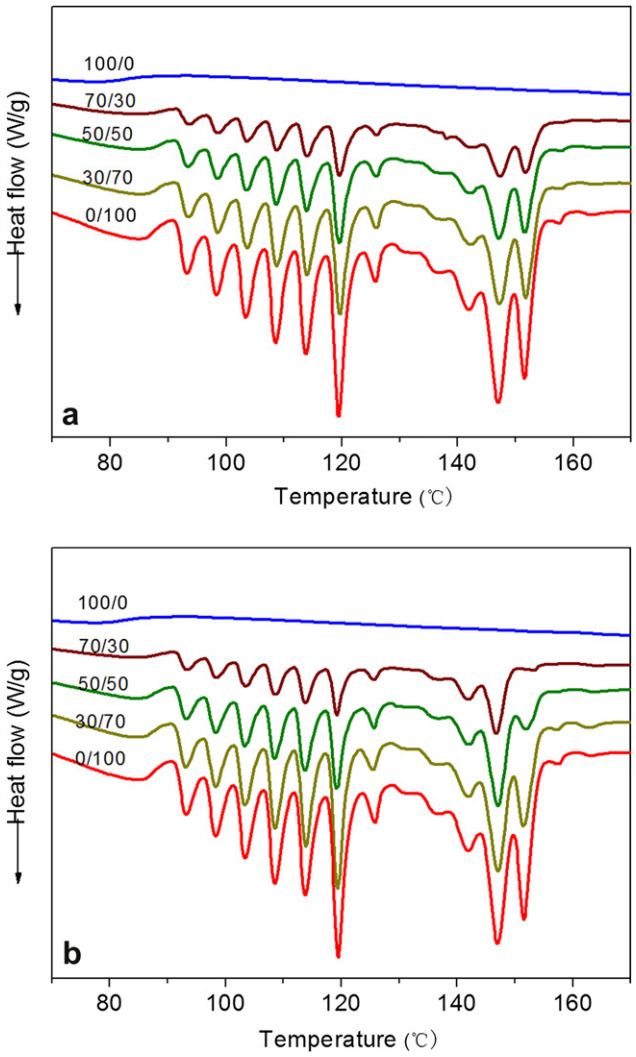

Fig. 11. DSC melting traces at a heating rate of 10 °C/min for blends of EPR and E*b*P fractions after SSA treatment for (a) unmixed samples and (b) solution-mixed samples.

which peak 1–3 is attributed to E*b*P fraction, and peak 4–5, to EPR fraction. However, only two melting peaks (labeled as 1′ and 2′) appear in the trace of solution-mixed sample. Furthermore, the melting peaks of the polypropylene crystals represented by Peak 1, 2 and 1′ seem different. Obviously, there exists some interaction between the EPR and E*b*P fraction in the solution-mixed samples, and the difference of the melting behavior between the unmixed and mixed samples may result from dilution effect. Here, to confirm this assumption, SSA technique is used to further investigate the interaction between the two fractions. Fig. 11 gives the melting traces of the unmixed and solution-mixed samples with various compositions after the SSA treatment. Due to the weak crystallization of EPR component, the temperature of SSA treatment is selected from 89 to 154 °C and no visible melting peaks of EPR fraction appear. Moreover, the melting peak at 152 °C for the solution-mixed blends is much weaker than that of the unmixed samples when their compositions are the same, especially for the samples with composition of 50/50 and 70/30. However, for the solution-mixed blends the melting peak at 147 °C is obviously stronger than that of the unmixed sample. In general, the crystals with the highest melting temperature are the one firstly crystallized in solidification course, and the nucleation at the beginning stage is rather difficult since the samples are subjected to a nonisothermal crystallization in the present research and the temperature is higher at earlier stages. As far as the poor crystallizing ability of the EPR fraction and the good compatibility between EPR and E*b*P are considered, we believed that the EPR fraction presents a strong dilution effect on the crystallization of E*b*P component and reduces the nucleation ability of E*b*P fraction, especially at the beginning stage. As a result, the amount of the crystals with the highest melting temperature remarkably decreases and the intensity of melting peak at 152 °C becomes lower. For other melting peaks, the dilution effect of EPR fraction can hardly be observed, because the corresponding crystals form at lower temperatures and the crystallization conditions are relatively milder (less harsh).

Based on the above results and discussion, it is suggested that the E*b*P component has a good compatibility with EPR and *i*PP, and the compatibilization effect of E*b*P component in IPC could be confirmed.

4. Conclusion

Based on the SEM, TEM analysis and chain structure model for the components of the IPC, a modified dispersed phase model for IPC with the core-shell structure has been proposed, in which the *i*PP component and EPR component were believed to be the matrix and the main dispersed phase respectively. Depending on its chain structure, the E*b*P component could form the core, the layer or the bridges connecting the core and E*b*P layer. The DMA results of IPC and its three fractions indicated that for both the IPC and its E*b*P fraction, there existed three obvious transition peaks corresponding to the glass transition of the polyethylene component, ethylene–propylene random copolymer component and polypropylene component. Due to the existence of polyethylene component in IPC, the T_g of EPR in IPC sample is obviously lower than that of EPR fraction. The glass transition behavior for the EPR/E*b*P blends implied that there existed a good compatibility between these two components. Moreover, the crystallization behavior of E*b*P/*i*PP and EPR/E*b*P blends indicated that for solution-mixed E*b*P/*i*PP blends there was co-crystallization between polypropylene chains in E*b*P fraction and in *i*PP fraction, and a dilute effect of EPR component on the crystallization of E*b*P fraction could be observed in solution-mixed EPR/E*b*P blends. Furthermore, it was suggested that the E*b*P component had a good compatibility with EPR and *i*PP, and could act as the compatibilizer in IPC.

Acknowledgements

This work was supported by National Basic Research Program of China (No. 2005CB623800), National Nature Science Foundation of China (Grant 50603023) and Joint Research Fund for Overseas Chinese Young Scholars (No. 50728302).

References

[1] Fan Z, Zhang Y, Xu J, Wang H, Feng L. Polymer 2001;42(13):5559–66.
[2] Cai H, Luo X, Ma D, Wang J, Tan H. Journal of Applied Polymer Science 1999;71(1):93–101.
[3] Xu J, Feng L, Yang S, Wu Y, Yang Y, Kong X. Polymer 1997;38(17):4381–5.
[4] Cheng HN, Lee GH. Macromolecules 1987;20(2):436–8.
[5] Fu Z, Fan Z, Zhang Y, Feng L. European Polymer Journal 2003;39(4):795–804.
[6] Hayashi T, Inoue Y, Chûjô R, Asakura T. Polymer 1988;29(10):1848–57.
[7] Mirabella FM, McFaddin DC. Polymer 1996;37(6):931–8.
[8] Hansen EW, Redford K, Øysæd H. Polymer 1996;37(1):19–24.
[9] Sun Z, Yu F, Qi Y. Polymer 1991;32(6):1059–64.
[10] Dong Q, Wang X, Fu Z, Xu J, Fan Z. Polymer 2007;48(20):5905–16.
[11] Tanem BS, Kamfjord T, Augestad M, Løvgren TB, Lundquist M. Polymer 2003;44(15):4283–91.
[12] Tan H, Xie K, Liu W, Hou B, Shangguan Y, Zheng Q. Acta Polymerica Sinica 2006;9:1106–11.
[13] Chen Y, Chen W, Yang D. Journal of Applied Polymer Science 2008;108(4):2379–85.
[14] Song S, Feng J, Wu P, Yang Y. Macromolecules 2009;42(18):7067–78.

[15] Tan H, Li L, Chen Z, Song Y, Zheng Q. Polymer 2005;46(10):3522–7.
[16] Shangguan Y, Tao L, Zheng Q. Journal of Applied Polymer Science 2007;106 (1):448–54.
[17] Zhang C, Shangguan Y, Chen R, Zheng Q. Journal of Applied Polymer Science, in press.
[18] Arnal ML, Sánchez JJ, Müller AJ. Polymer 2001;42(16):6877–90.
[19] Arnal ML, Balsamo V, Ronca G, Sanchez A, Muller AJ, Canizales E, et al. Journal of Thermal Analysis and Calorimetry 2000;59(1–2):451–70.
[20] Zhu H, Monrabal B, Han CC, Wang D. Macromolecules 2007;41(3):826–33.
[21] Muller AJ, Arnal ML. Progress in Polymer Science 2005;30(5):559–603.
[22] Jang BZ, Uhlmann DR, Sande JBV. Journal of Applied Polymer Science 1985;30 (6):2485–504.
[23] Nitta K, Kawada T, Yamahiro M, Mori H, Terano M. Polymer 2000;41 (18):6765–71.
[24] Shangguan Y, Zhang C, Xie Y, Chen R, Jin L, Zheng Q. Polymer 2010;51(2):500–6.
[25] Zheng Q, Shangguan Y, Yan S, Song Y, Peng M, Zhang Q. Polymer 2005;46 (9):3163–74.
[26] Shangguan Y, Song Y, Zheng Q. Polymer 2007;48(15):4567–77.
[27] Lohse DJ, Datta S, Kresge EN. Macromolecules 1991;24(2):561–6.
[28] Lohse DJ, Fetters LJ, Doyle MJ, Wang HC, Kow C. Macromolecules 1993;26 (13):3444–7.
[29] Silvestre C, Cimmino S, Triolo R. Journal of Polymer Science Part B: Polymer Physics 2003;41(5):493–500.
[30] Zhang M, Duhamel J. Macromolecules 2007;40(3):661–9.